

1

# 2 **The Aerosol Module in the Community Radiative Transfer Model** 3 **(v2.2 and v2.3): accounting for aerosol transmittance effects on the** 4 **radiance observation operator**

5 Cheng-Hsuan (Sarah) Lu<sup>1,2</sup>, Quanhua Liu<sup>3</sup>, Shih-Wei Wei<sup>1,2</sup>, Benjamin T. Johnson<sup>4</sup>, Cheng Dang<sup>1</sup>,  
6 Patrick G. Stegmann<sup>4</sup>, Dustin Grogan<sup>2</sup>, Guoqing Ge<sup>5,6</sup>, Ming Hu<sup>6</sup>, and Michael Lueken<sup>7,8</sup>

7  
8 <sup>1</sup>Joint Center for Satellite Data Assimilation, Boulder, CO, USA

9 <sup>2</sup>Atmospheric Sciences Research Center, University at Albany, Albany, NY, USA

10 <sup>3</sup>Center for Satellite Applications and Research, NOAA/NESDIS, College Park, MD, USA

11 <sup>4</sup>Joint Center for Satellite Data Assimilation, College Park, MD, USA

12 <sup>5</sup>Cooperative Institute for Research in Environmental Sciences, CU Boulder, CO, USA

13 <sup>6</sup>Global System Laboratory, NOAA, Boulder, CO, USA

14 <sup>7</sup>I.M. Systems Group, Inc., Rockville, MD, USA

15 <sup>8</sup>Environmental Modeling Center, NOAA/NWS/NCEP, College Park, MD, USA

16  
17 *Correspondence to:* Cheng-Hsuan Lu ([clu@ucar.edu](mailto:clu@ucar.edu); [clu4@albany.edu](mailto:clu4@albany.edu))

## 18 **Abstract**

19 The Community Radiative Transfer Model (CRTM), a sensor-based radiative transfer model, has been used within the  
20 Gridpoint Statistical Interpolation (GSI) system for directly assimilating radiances from infrared and microwave sensors. We  
21 conducted numerical experiments to illustrate how including aerosol radiative effects in CRTM calculations changes the GSI  
22 analysis. Compared to the default aerosol-blind calculations, the aerosol influences reduced simulated brightness temperature  
23 (BT) in thermal window channels, particularly over dust-dominant regions. A case study is presented, which illustrates how  
24 failing to correct for aerosol transmittance effects leads to errors in meteorological analyses that assimilate radiances from  
25 satellite IR sensors. In particular, the case study shows that assimilating aerosol-affected BTs significantly affects analyzed  
26 temperatures in the lower atmosphere across several regions of the globe. Consequently, a fully-cycled aerosol-aware  
27 experiment improves 1-5 day forecasts of wind, temperature, and geopotential height in the tropical troposphere and Northern  
28 Hemisphere stratosphere. Whilst both GSI and CRTM are well documented with online user guides, tutorials and code  
29 repositories, this article is intended to provide a joined-up documentation for aerosol absorption and scattering calculations in  
30 the CRTM and GSI. It also provides guidance for prospective users of the CRTM aerosol option and GSI aerosol-aware  
31 radiance assimilation. Scientific aspects of aerosol-affected BT in atmospheric data assimilation are briefly discussed.

## 32 **1 Introduction**

33 An accurate and computationally efficient radiative transfer model is essential in radiance assimilation for supporting weather  
34 prediction, physical retrievals for satellite environmental data records, and inter-comparison among remote sensing sensors.  
35 The Community Radiative Transfer Model (CRTM) is a sensor-based radiative transfer model (Weng, 2007; Han et al., 2007).  
36 It was primarily designed for computing satellite radiances and has been used within the Gridpoint Statistical Interpolation  
37 (GSI, Wu et al., 2002; Kleist et al., 2009) system for directly assimilating radiances from infrared (IR) and microwave (MW)  
38 sensors. Specifically, clear-sky radiance calculations are carried out within the CRTM given the atmospheric scattering and  
39 absorption profile, surface emissivity and reflectivity, and source functions. For cloudy radiance simulations (Stegmann et al.,  
40 2018), vertical profiles of hydrometeor variables (e.g., cloud liquid water path and ice water path) are also required. Note that  
41 CRTM is not designed to describe longwave and shortwave broadband radiative transfer for general circulation model  
42 applications. Instead, it is developed to support satellite radiance data assimilation and satellite retrieval development.

43  
44 Past studies have demonstrated that aerosols significantly impact the simulation of brightness temperature (BT) in the IR  
45 channels. BT is “a descriptive measure of radiation in terms of the temperature of a hypothetical blackbody emitting an  
46 identical amount of radiation at the same wavelength” (American Meteorological Society, 2012). A reduction in retrieved BT  
47 of 2-4 K in the atmospheric window region due to a strong dust outbreak was reported during the Saharan Dust Experiment  
48 (SHADE) campaign (Highwood et al., 2003). Pierangelo et al. (2004) and Peyridieu et al. (2009) showed that the dust cooling  
49 effects may reach 3 K in tropical atmospheric conditions depending on the dust burden. Diaz et al. (2001) found that there is  
50 a significant increase in the errors of sea surface temperature (SST) retrievals in the presence of enhanced aerosol loading in  
51 the atmosphere. The dust effects on satellite derived SST are constrained by accounting for dust absorption (Weaver et al.,  
52 2003), applying a dust correction scheme (Nalli and Stowe, 2002; Merchant et al., 2006), or removing dust-contaminated  
53 observations (Divakarla et al., 2012).

54  
55 The impact of aerosol-affected BTs on the meteorological analysis fields has also been investigated. Wei et al. (2021a) used  
56 the Global Data Assimilation System (GDAS) to assess the aerosol impact on the GDAS analysis. To do this, two GDAS  
57 experiments were conducted: a control cycled experiment, where aerosol transmittance effects are not considered, and an  
58 offline non-cycled experiment, where aerosol transmittance effects are considered in the BT calculations. The offline  
59 experiment uses identical observations and first guesses as the control experiment and thus the response of atmospheric analysis  
60 to aerosol-aware radiance calculations can be clearly demonstrated. The experimental setup in Wei et al. (2021a) followed the  
61 methodology presented in Kim et al. (2018), which is based on the Goddard Earth Observing System (GEOS)-atmospheric  
62 data assimilation system (ADAS). Note that GEOS-ADAS and GDAS both used GSI and CRTM, although the version and  
63 configuration differed. The studies by Kim et al. (2018) and Wei et al. (2021a) reported that: (i) a considerable cooling effect  
64 on simulated BT when aerosols are considered; (ii) including aerosol transmittance effects in the BT calculation improves the

65 fit to observations over the dust-laden regions, and (iii) the offline aerosol-aware experiment produces warmer analyzed SST  
66 (0.3 - 0.5 K) over the Atlantic Ocean. Wei et al. (2021a) also reported a warmer analysed lower atmosphere (0.15 K) over  
67 Africa and the central Atlantic Ocean in the offline aerosol-aware experiment.

68

69 The experiments conducted in Kim et al. (2018) and Wei et al. (2021a) were based on the application of the CRTM aerosol  
70 absorption and scattering routines. While aerosol absorption and scattering options are available from CRTM version 2.2  
71 onwards; to our knowledge, the documentation of the CRTM aerosol module (Liu and Lu, 2016) has yet to be updated. Here  
72 we presented a joined-up documentation for aerosol absorption and scattering calculations in the CRTM and GSI. In addition,  
73 we provide guidance for prospective users of running aerosol-affected GSI analysis. Scientific aspects of aerosol-affected BT  
74 in atmospheric data assimilation are also briefly discussed.

## 75 **2 GSI and CRTM**

76 Below, we provide a brief introduction to the GSI in section 2.1 and a description of the CRTM aerosol option in section 2.2.  
77 In section 2.3, a description of running aerosol-aware GSI analysis is given.

### 78 **2.1 GSI**

79 The multi-partner-developed GSI is an incremental three-dimensional variational (3D-Var) data assimilation system (Wu et  
80 al., 2002; Kleist et al. 2009). GSI, alone or combined with an ensemble system, has been used widely by modelling centers  
81 and the research community for a range of research and applications. For instance, it is used operationally by the National  
82 Oceanic and Atmospheric Administration (NOAA)/National Centers for Environmental Prediction (NCEP) for medium-range  
83 weather forecast. It is also used by the National Aeronautics and Space Administration (NASA)/Global Modeling and  
84 Assimilation Office (GMAO) for recent production of the Modern-Era Retrospective Analysis for Research and Applications,  
85 version 2 (MERRA-2; Gelaro et al., 2017). The community version of the GSI system has been supported and maintained by  
86 the Developmental Testbed Center (DTC; <http://www.dtcenter.org>). Note that DTC is scheduled to cease all activities  
87 supporting the GSI user community by the end of December 2021. However, community GSI-related assets (website, forum,  
88 and repository) built by DTC will remain available to and usable by the community.

89

90 GSI can assimilate a wide range of observations, including conventional observations (such as radiosonde observations), radar  
91 data, satellite retrievals (for example global positioning system (GPS) radio occultation sounding data), satellite radiance data,  
92 etc. For IR satellite instruments, GSI has the capability to assimilate radiances from Advanced Infrared Sounder (AIRS) on  
93 AQUA, Infrared Atmospheric Sounding Interferometer (IASI) on METOP-A and METOP-B, Cross-track Infrared Sounder  
94 (CrIS) on S-NPP, High resolution Infrared Radiation Sounder (HIRS) on METOP-A, METOP-B, and NOAA-19, Advanced  
95 Very High Resolution Radiometer (AVHRR) on NOAA-18 and METOP-A, Spinning Enhanced Visible and Infrared Imager

96 (SEVIRI) on M08 and M10, and Geostationary Operational Environmental Satellite (GOES) Sounders (sndrD1, sndrD2,  
97 sndrD3, and sndrD4) on GOES-15. A comprehensive list of all observations assimilated and monitored by GDAS can be found  
98 at the webpage for “Observational Data Processing at NCEP” ([https://www.emc.ncep.noaa.gov/emc/pages/infrastructure/obs-  
100 data-processing.php](https://www.emc.ncep.noaa.gov/emc/pages/infrastructure/obs-<br/>99 data-processing.php)).

101 Despite the broad applications of GSI, the publicly released version handles only clear-sky radiances for IR sensors. Without  
102 correcting for aerosol transmittance effects, systematic biases may be introduced into the meteorological analysis fields when  
103 observations affected by aerosols are assimilated. The aerosol-aware option (discussed in section 2.2) reduces such errors by  
104 enabling aerosols to influence GSI's radiance observation operator, CRTM, which calculates the BT and Jacobians (radiance  
105 1<sup>st</sup> derivative). This option, however, may fluctuate the amount of observations assimilated in GSI because the quality control  
106 (QC) algorithm screens out observations based on measured BTs and aerosol-free simulated BTs. Thus, an improved QC  
107 algorithm is needed to fully exploit radiance measurements under all sky conditions. The technical issues regarding the QC  
108 procedure have been discussed in Kim et al. (2018) and Wei et al. (2021 a).

## 109 **2.2 CRTM aerosol module**

110 The CRTM, a one-dimensional radiative transfer model (Liu and Weng, 2006), is developed at the U.S. Joint Center for  
111 Satellite Data Assimilation (JCSDA) with algorithm and software input from JCSDA collaborating research institutions. The  
112 CRTM is composed of four modules, which include gaseous transmittance, surface emission and reflection, cloud and aerosol  
113 absorption and scattering, and a solver for radiative transfer (Han et al., 2006). Given an atmospheric profile of temperature,  
114 cloud and surface properties, and gaseous constituents and aerosol concentrations, the CRTM is called within the GSI to  
115 calculate BTs for satellite sensors from IR sounders to MW imagers. Here, we describe the aerosol scattering and absorption  
116 scheme in CRTM version 2. We refer the readers to Han et al. (2006) for the full details regarding CRTM version 1.

117  
118 Absorption by atmospheric trace gases, such as water vapor and carbon dioxide, is parameterized using the Optical Depth in  
119 Absorber Space (ODAS) and the Optical Depth in Pressure Space (ODPS) algorithms (Chen et al., 2012), which are based on  
120 rigorous line-by-line calculations from the Line-By-Line Radiative Transfer Model (LBLRTM, Clough et al., 1992). Scattering  
121 and absorption by aerosols are calculated based on pre-computed lookup tables containing aerosol optical properties, including  
122 extinction coefficient, single-scattering albedo, asymmetry factor, and phase function coefficients. Operationally, given aerosol  
123 types, radius, concentration and ambient relative humidity, CRTM generates aerosol optical profiles that the radiative transfer  
124 solver requires for multi-scattering simulations and radiance calculations. The CRTM version 2.2 and 2.3 contain the optical  
125 look-up table that is based on the Goddard Chemistry Aerosol Radiation and Transport (GOCART, Chin et al., 2002; Colarco  
126 et al, 2010) model for the spectrum from ultraviolet to IR. The effect of aerosols on MW sensors is not considered yet because  
127 the impact of aerosols on MW radiance is usually very small, given aerosols size is generally much smaller than MW  
128 wavelengths (Petty, 2006). There are ongoing and planned CRTM development efforts to incorporate more aerosol optical

129 tables (such as the Community Multiscale Air Quality model, CMAQ). With the expansion of the aerosol schemes, a new  
 130 releasing and versioning system for optical tables is essential and currently under discussion. This article, however, discusses  
 131 mainly the GOCART model, which is the default aerosol scheme in the CRTM version 2.

132

133 The GOCART model (Chin et al., 2002; 2014), a bulk aerosol scheme, simulates major tropospheric aerosol components,  
 134 including dust, sea salt, black carbon (BC), organic carbon (OC) and sulfate. It is one of the most widely used aerosol modules  
 135 in the Weather Research and Forecasting model coupled with Chemistry (WRF-Chem; see Ukhov et al. (2021) and references  
 136 therein). It is used in the GEOS framework at GMAO for near-real-time aerosol forecasts (Colarco et al., 2010) as well as in  
 137 MERRA reanalysis (Bucharad et al., 2015) and MERRA-2 reanalysis (Randles et al., 2017). It is also implemented in the Global  
 138 Forecast System (GFS) framework at NCEP (Lu et al., 2016; Wang et al., 2018; Zhang et al., 2021) for near-real-time global  
 139 aerosol forecasts.

140

141 When GOCART was selected as the aerosol module within WRF-Chem, it was configured with fourteen GOCART aerosol  
 142 species (Liu et al., 2011): sulfate; hydrophobic and hydrophilic OC and BC; sea salt in four particle size bins (with radii of  
 143 0.1-0.5, 0.5-1.5, 1.5-5, and 5-10  $\mu\text{m}$ ) and dust particles in five particle size bins (with radii of 0.1-1.0, 1.0-1.8, 1.8-3, 3-6, and  
 144 6-10  $\mu\text{m}$ ). A default CRTM lookup-table has been used for pre-calculated aerosol optical property parameters for the fourteen  
 145 GOCART aerosol species (Liu et al., 2007; Liu and Lu, 2016). We assume that the particles are spherical and externally mixed.  
 146 We also assume lognormal size distributions for sulfate and carbonaceous aerosols as well as for each sea salt and dust bin.  
 147 The lognormal size distribution for N particles can be expressed as follows (d'Almeida et al., 1991),

$$148 \quad n(\ln r) = \frac{N}{\sqrt{2\pi} \ln(\sigma_g)} \exp\left[-\frac{1}{2} \left(\frac{\ln r - \ln r_g}{\ln(\sigma_g)}\right)^2\right], \quad (1)$$

149 where  $r$  is a radius,  $r_g$  the geometric median radius, and  $\sigma_g$  the geometric mean standard deviation. The  $k^{\text{th}}$  moment of the  
 150 distribution can be expressed as follows (Binkowski and Roselle, 2003),

$$151 \quad M_k = \int_{-\infty}^{\infty} r^k n(\ln r) d\ln(r) = r_g^k \exp\left[\frac{k^2}{2} \ln^2(\sigma_g)\right]. \quad (2)$$

152 where  $M_0$  is the number N of aerosol particles, and  $M_2$  and  $M_3$  are proportional to the total particulate surface area and volume,  
 153 respectively. Thus, the effective radius ( $r_{\text{eff}}$ ) can be defined as

$$154 \quad r_{\text{eff}} = \frac{M_3}{M_2} = r_g \exp\left[\frac{5}{2} \ln^2(\sigma_g)\right]. \quad (3)$$

155

156 Table 1 lists the GOCART size parameters (particle density, effective radius, and geometric standard deviation) and refractive  
 157 indices at 550 nm used in CRTM version 2. The optical properties of each aerosol species are computed based on Mie scattering  
 158 theory. Hydrophilic aerosol particle size increases as relative humidity (RH) of the ambient atmosphere increases. Therefore,

159 the water content in aerosol needs to be considered when calculating the refractive index. The effective radius growth factor  
 160 for hygroscopic aerosols may be theoretically calculated or obtained from a pre-calculated look-up table (d’Almeida et al.,  
 161 1991). In this study, the hygroscopic growth factor used for the GOCART model (Chin et al., 2002) is adopted and given in  
 162 Table 2. Once the growth factor  $a_g$  is evaluated, the refractive index  $n_r$  for the hygroscopic aerosol can be calculated using a  
 163 volume mixing method as:

$$164 \quad n_r = n_w + (n_o - n_w) \times a_g^3 \quad (4)$$

165 where  $n_o$  and  $n_w$  are the refractive indices for dry aerosols and water, respectively. We adopt the refractive index  $n_o$  from the  
 166 Optical Properties of Aerosols and Clouds (OPAC) dataset (Hess et al. 1998), while the water refractive index is given by  
 167 (Hale and Querry, 1973).

168  
 169 **Table 1.** Goddard Chemistry Aerosol Radiation and Transport (GOCART) size distribution parameters and refractive indices  
 170 at 550 nm for dry aerosols.

Aerosol type	Density [g cm <sup>-3</sup> ]	Effective radius $r_{\text{eff}}$ [μm]	Standard deviation $\sigma$ [μm]	Refractive index real part $n(\lambda)$	Refractive index imaginary part $k(\lambda)$
Sulfate	1.7	0.242	2.03	1.43	$1.00 \times 10^{-8}$
OC1 (hydrophobic)	1.8	0.087	2.20	1.53	$6.00 \times 10^{-3}$
OC2 (hydrophilic)	1.8	0.087	2.20	1.53	$6.00 \times 10^{-3}$
BC1 (hydrophobic)	1.0	0.036	2.0	1.75	$4.40 \times 10^{-1}$
BC2 (hydrophilic)	1.0	0.036	2.0	1.75	$4.40 \times 10^{-1}$
SeaSalt1 (size range)	2.2	0.3	2.03	1.50	$1.00 \times 10^{-8}$
SeaSalt2	2.2	1.0	2.03	1.50	$1.00 \times 10^{-8}$
SeaSalt3	2.2	3.25	2.03	1.50	$1.00 \times 10^{-8}$
SeaSalt4	2.2	7.5	2.03	1.50	$1.00 \times 10^{-8}$
Dust1 (size range)	2.6	0.65	2.0	1.53	$5.50 \times 10^{-3}$
Dust2	2.6	1.4	2.0	1.53	$5.50 \times 10^{-3}$
Dust3	2.6	2.4	2.0	1.53	$5.50 \times 10^{-3}$
Dust4	2.6	4.5	2.0	1.53	$5.50 \times 10^{-3}$
Dust5	2.6	8.0	2.0	1.53	$5.50 \times 10^{-3}$

171  
 172 **Table 2.** Hygroscopic aerosol growth factor  $a_g$  as a function of the ambient relative humidity (RH).

RH(%)	0	50	70	80	90	95	99
Sulfate	1.0	1.4	1.5	1.6	1.8	1.9	2.2
Organic Carbon	1.0	1.2	1.4	1.5	1.6	1.8	2.2
Black Carbon	1.0	1.0	1.0	1.2	1.4	1.5	1.9

Sea Salt	1.0	1.6	1.8	2.0	2.4	2.9	4.8
----------	-----	-----	-----	-----	-----	-----	-----

173

174 The GOCART model used by GMAO and NCEP for aerosol forecast and reanalysis has evolved to use 5 sea salt size bins  
 175 (with radii of 0.03-0.1, 0.1-0.5, 0.5-1.5, 1.5-5, and 5-10  $\mu\text{m}$ ). The first sub-micron sea salt bin was added to facilitate optical  
 176 properties and aerosol-cloud interaction studies (Colarco et al., 2010), but was excluded from the previous GOCART versions  
 177 as well as the WRF-Chem GOCART model. While GMAO’s GEOS and NCEP’s GFS contain fifteen GOCART aerosol  
 178 species, the CRTM aerosol module has also not yet been modified to include the new added sub-micron sea salt bin (see Table  
 179 1). To overcome this discrepancy, the latest GSI/CRTM release (i.e., GSI 3.7 and CRTM 2.3) combines the mixing ratios from  
 180 the two sub-micron sea salt bins in order to use the aerosol optical property parameters from the original GOCART model.  
 181 This limitation is acknowledged in this article and will be addressed in a future CRTM release (see section 4).

182

183 While the CRTM is primarily designed for computing satellite radiances, an additional module was added to CRTM by Liu  
 184 and Lu (2016) to compute aerosol optical depth (AOD). This CRTM-AOD module enables the GSI system to assimilate AOD  
 185 observations (Liu et al., 2011; Schwartz et al., 2012; Pagowski et al., 2014). This article, however, is focused on the observation  
 186 operator for radiance, and we refer the reader to Pagowski et al. (2014) for the description of the AOD observation operator  
 187 and GSI AOD data assimilation.

### 188 **2.3 Running aerosol-aware GSI analysis**

189 The operational version of GSI maintained by NOAA/NCEP Environmental Modeling Center (EMC) is utilized in the present  
 190 study. Its source code and associated static files are distributed through the GitHub repository (<https://github.com/NOAA-EMC/GSI>). An open-access archive of source code and data is described in Code and Data Availability. To run the GSI  
 191 analysis, the reader can refer to the user guide for GSI v3.7 (the latest released version as of April 2021), which is available at  
 192 [https://dtcenter.ucar.edu/com-GSI/users/docs/users\\_guide/html\\_v3.7/index.html](https://dtcenter.ucar.edu/com-GSI/users/docs/users_guide/html_v3.7/index.html). In addition, an online tutorial is available at  
 193 [https://dtcenter.ucar.edu/com-GSI/users/tutorial/online\\_tutorial/index\\_v3.7.php](https://dtcenter.ucar.edu/com-GSI/users/tutorial/online_tutorial/index_v3.7.php). For CRTM, the user guide and tutorials can  
 194 be found at <https://www.jcsda.org/jcsda-project-community-radiative-transfer-model>. Thus, only a brief description of  
 195 aerosol-affected BT calculations is given.

197

198 A regression test “global\_C96\_fv3aerorad” has been introduced into NOAA/EMC GSI code repository (pull request #32) to  
 199 assure the functionality of aerosol-aware BT derivations in GSI/CRTM works as expected. This regression test uses a sample  
 200 background file taken from the aerosol member of the Global Ensemble Forecast System (GEFS-Aerosol; Zhang et al., 2021).  
 201 All fifteen GOCART aerosol species are passed along to the CRTM. In addition to the background file, a user needs to modify  
 202 the configuration files, anavinfo and satinfo, in the “fix” directory. The anavinfo file is the information file to set control and  
 203 analysis variables. The satinfo file is the information file to specify satellite channels to be assimilated and associated  
 204 parameters. For an aerosol-aware experiment where aerosol absorption and scattering are included in BT calculations, aerosol

205 species are specified in the “chem\_guess” section of anavinfo and sensors and channels are set to 1 in the “iaerosol” column  
206 of satinfo. The reader can refer to the fv3aerorad\_satinfo.txt and anavinfo\_fv3aerorad for the aerosol-aware configuration. The  
207 corresponding namelist (gsiparm.anl) can be found at the “global\_C96\_fv3aerorad” section (line 2931–3046) in  
208 regression\_namelists.sh under the “regression” directory. It should be noted that the namelist variable, “lread\_ext\_aerosol”,  
209 determines how GSI ingests the aerosol information from background files or external files.

### 210 **3. Numerical Results**

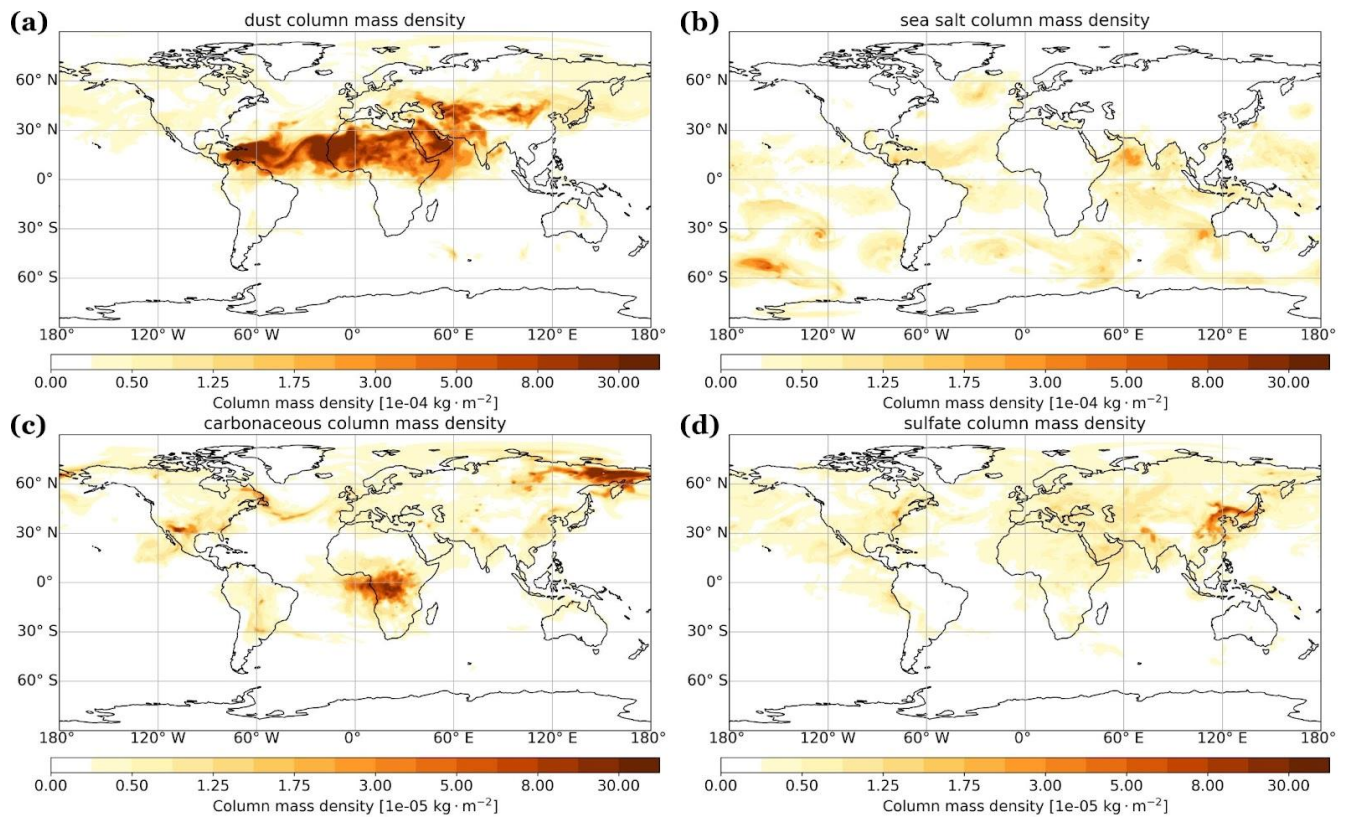
#### 211 **3.1 Aerosol impacts on BT calculations**

212 To illustrate how an aerosol transmittance correction is required within satellite radiances assimilated into meteorological data  
213 assimilation systems, we present a detailed analysis of a single-cycle GSI experiment (the AER experiment) using GOCART  
214 fields from MERRA-2 on 12Z June 22, 2020. This time is chosen because it captures a strong Saharan dust event that covers  
215 the trans-Atlantic region. A baseline GSI experiment (the CTL experiment) with the anavinfo and satinfo resource files reverted  
216 back to the default aerosol-blind configuration was also conducted. Both experiments used the same first-guess fields and  
217 assimilated identical conventional and satellite observations within a  $\pm 3$ -hour assimilation window. In AER, the aerosol  
218 transmittance effects were only considered in the CRTM simulation for IR sensors.

219  
220 Figure 1 shows the global aerosol column mass density distribution from MERRA-2 during 12Z June 22, 2020. The panels a,  
221 b, c, and d depict dust, sea salt, carbonaceous and sulfate, respectively. Dust plumes spread over northern Africa, the tropical  
222 Atlantic Ocean, the Middle East, and northwestern China. Wind-driven sea salt aerosols are seen over tropical and southern  
223 hemisphere oceans. Carbonaceous and sulfate aerosols mainly appear in areas with extensive biomass burning and fuel  
224 combustion activities (note one order smaller than dust and sea salt). The overall aerosol loading is dominated by mineral dust.  
225 Wu et al. (2020) evaluated the dust spatiotemporal variations of MERRA-2 against satellite observations and global model  
226 simulations. They found that MERRA-2 agrees well with satellite observations due to the assimilation of satellite AOD. But  
227 in North America and the Arctic, the dust burden in MERRA-2 is much larger than those in other models despite having similar  
228 dust emissions fluxes. The high dust burden over these regions is due to higher mass fraction of fine dust and enhanced dust  
229 transport. Furthermore, Bullard et al. (2016) reported that large gaps exist in our understanding of basic characteristics of high-  
230 latitude dust sources. This highlights the importance of representing aerosol emissions, transport, removal, and size distribution  
231 in global models in correctly simulating aerosol spatiotemporal distributions.

232





233

234

**Figure 1.** Aerosol column mass density ( $\text{kg m}^{-2}$ ) from MERRA-2 on 12Z June 22, 2020: (a) dust, (b) sea salt, (c) carbonaceous, and (d) sulfate.

235

236

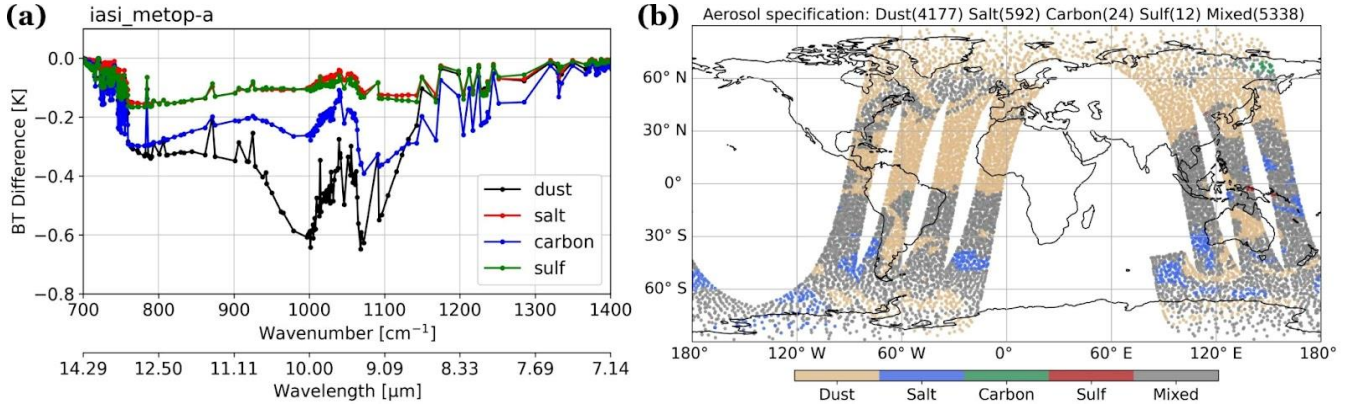
237

Figure 2a shows the first-guess BT differences of IASI onboard METOP-A between the two experiments (AER – CTL) in the IR atmospheric window channels over dust, sea salt, carbonaceous and sulfate dominant regions. The stratification criterion for each type is where the fraction of column mass density of dominant species, from MERRA-2, is larger than 0.65 (shown in Fig. 2b). Figure 2a shows that dust aerosols generate the stronger cooling effects, about 0.7 K at the thermal IR window region ( $\sim 10 \mu\text{m}$ ), than other species. The importance of correcting for aerosol transmittance effects within BT algorithms has been reported in previous studies (Sokolik, 2002; Weaver et al., 2003; Pierangelo et al., 2004; Matricardi, 2005; Merchant et al., 2006; Kim et al., 2018; Wei et al., 2021a). Table 3 describes the range and the average of total aerosol column mass density over the regions with different dominant aerosol species. It shows that the total loading of aerosols is similar over the dust and carbonaceous aerosols dominated regions. This indicates that the stronger cooling effects by dust aerosol on BT in the IR window region is not due to stronger loading. Note that in the northern hemisphere, the high-latitude region is characterized as dust-dominant except for the Russian Far East in MERRA-2 (Figure 2b). While anomalous or erroneous modeled aerosol loading may bias the results, the finding that dust has the largest impact on the BTs simulations, reported in this study and

248

249 previous studies, remains unchanged. Therefore, we focus our remaining analysis on dust over Tropical Africa and the Mid-  
 250 Atlantic.

251  
 252



253  
 254  
 255  
 256  
 257

**Figure 2.** (a) The differences (AER-CTL) of first-guess brightness temperatures in the IR window region of IASI onboard METOP-A. (b) The corresponding regions dominated by different aerosol species from the 12Z June 22, 2020. The data counts for each species are labelled in panel (b).

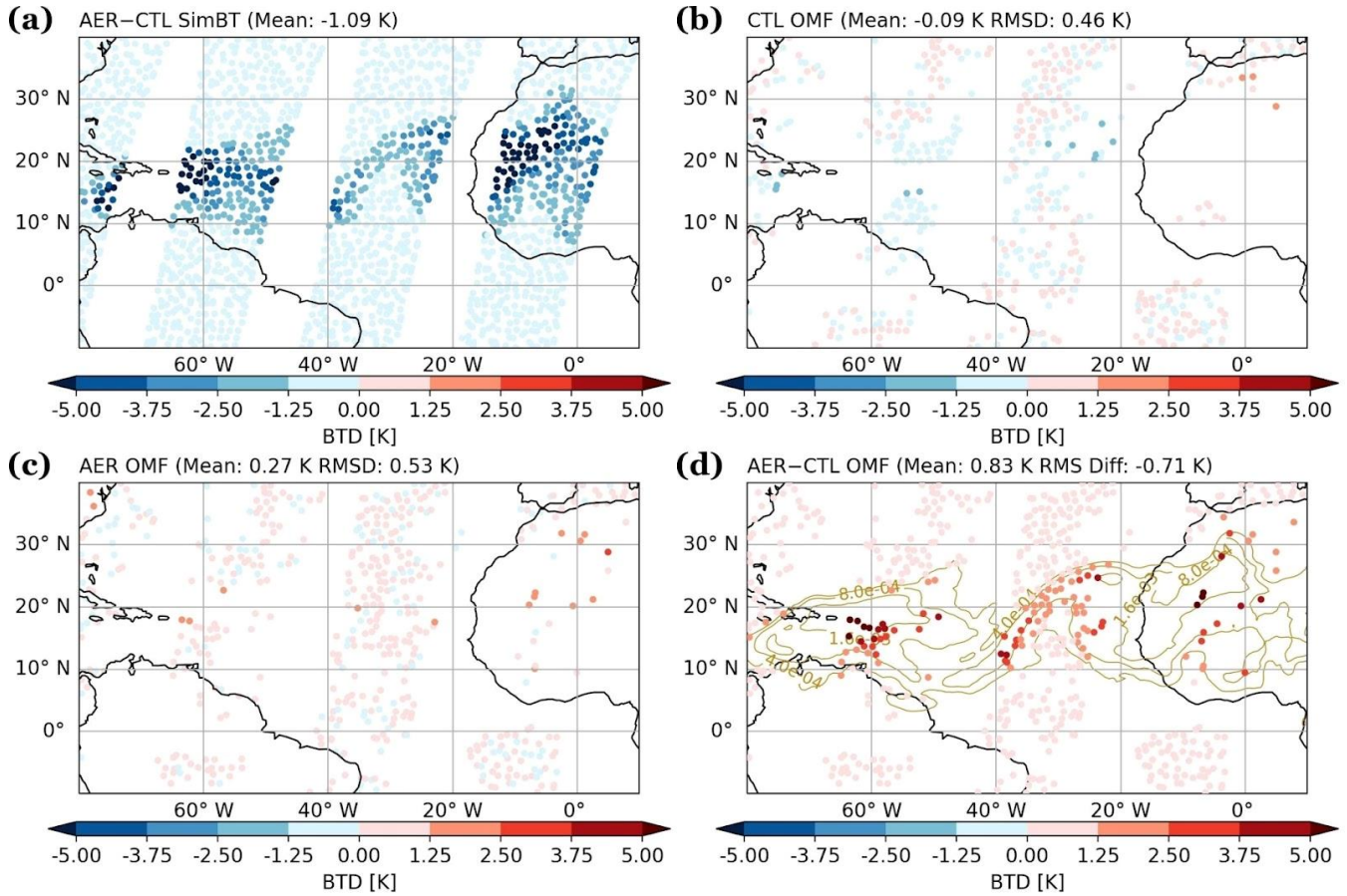
**Table 3.** The range of aerosol column mass density ( $\text{kg}/\text{m}^2$ ) from MERRA-2 at the regions dominated by different aerosol species (fraction over 0.65) of IASI onboard METOP-A at the cycle of 12Z June 22, 2020.

Dominant aerosol species	Column mass density ( $\text{kg}/\text{m}^2$ )				
	Minimum	Maximum	Mean	Median	SD
Dust	2.69e-06	2.88e-03	1.76e-04	4.20e-05	3.59e-04
Sea salt	4.91e-06	4.01e-05	1.68e-05	1.59e-05	6.15e-06
BC+OC	1.04e-05	6.07e-04	1.76e-04	1.52e-04	1.20e-04
Sulfate	6.45e-06	9.53e-05	2.15e-05	1.28e-05	2.46e-05

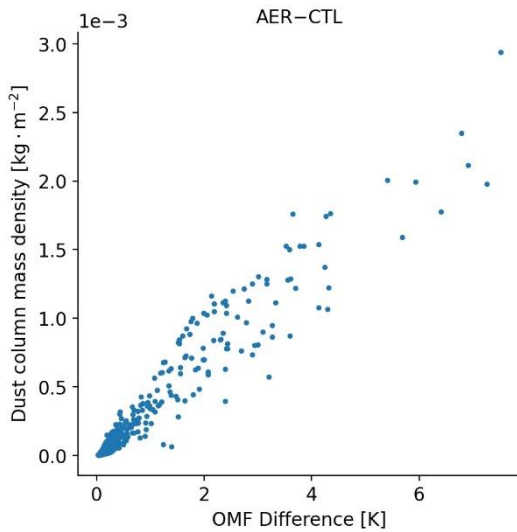
260  
 261  
 262  
 263  
 264  
 265  
 266

Figure 3 displays the AER - CTL difference in the simulated BTs and their respective first-guess departures (observed minus first guess, OMF) calculated at the 10.39  $\mu\text{m}$  channel from IASI onboard METOP-A. The Figure focuses on North Africa and the trans-Atlantic region, where a large dust plume spans the region. Significant aerosol cooling ( $\sim 4$  K) in BT was found in the aerosol-aware experiment (Fig. 3a) due to the large plume. Comparing the first guess departures from CTL and AER experiments (Fig. 3b and 3c) shows that OMFs for AER are warmer than CTL (cf. 0.27 K vs. -0.09 K). Note that some observations assimilated in CTL were rejected in AER (near 55° W and 15° N) and vice versa (near 65° W and 15° N, and

267 over Africa). This feature suggests that the quality control has been influenced by including aerosol transmittance effects in  
 268 CRTM. Over the trans-Atlantic region, the aerosol-aware experiment assimilated several observations with larger first-guess  
 269 departures located in the strong dust plume (Fig. 3d). Figure 4 presents the scatter plot of dust column mass density versus  
 270 OMF differences (AER - CTL) for these data points assimilated in AER on 12Z June 22, 2020. The data points with large  
 271 OMF differences are corresponding to the areas with higher dust loading. Nevertheless, when considering aerosol information,  
 272 the root-mean-square first-guess departures decreased 0.08 K globally and 0.42 K over the trans-Atlantic region at this channel  
 273 (not shown here). This implies that simulated BTs in the aerosol aware run are in better agreement with the observations.  
 274  
 275



276  
 277 **Figure 3.** (a) Simulated BT differences (AER - CTL), (b) bias-corrected OMF from the CTL experiment, (c) bias-corrected  
 278 OMF from the AER experiment, and (d) OMF differences (AER - CTL) for 10.39  $\mu\text{m}$  channel of IASI onboard METOP-A.  
 279 All the data are from the analysis cycle on 12Z June 22, 2020. Contours of total column mass density from MERRA-2 are  
 280 plotted in panel (d).



281

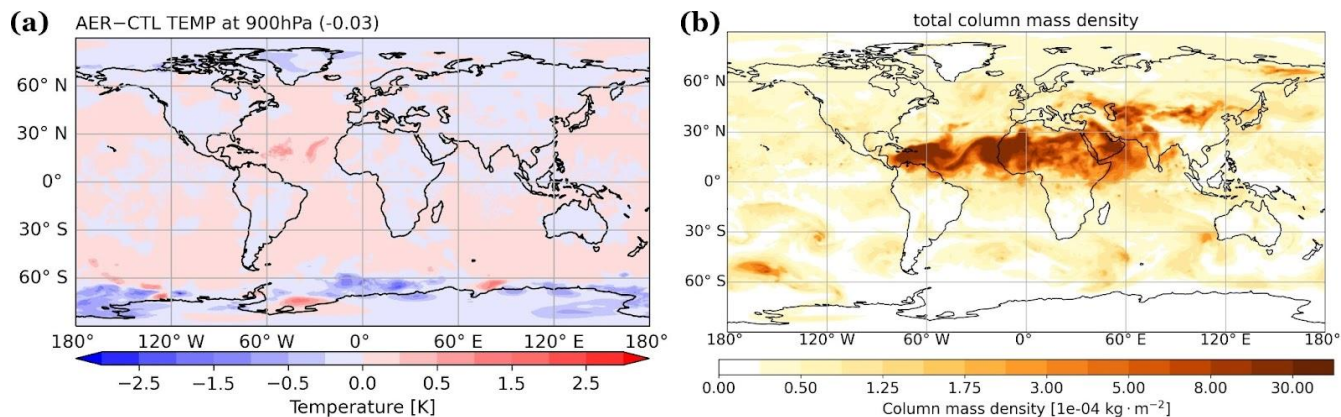
282 **Figure 4.** The scatter plot of dust column mass density from MERRA-2 against the first-guess departure differences (AER –  
 283 CTL) assimilated in AER experiment (without bias correction) on 12Z June 22, 2020.

284

285 Figure 5 shows (a) the global differences in analyzed temperature at 900 hPa between the two experiments and (b) the total  
 286 aerosol column mass density incorporated in the GSI/CRTM system. When aerosol transmittance effects are considered in the  
 287 BT calculations, the air temperatures are not only adjusted over aerosol-laden regions but also across the globe. The impact is  
 288 shown outside aerosol-active regions, which could be attributed to the change from the spatial correlation in the GSI  
 289 background error covariance. Over the trans-Atlantic region where the dust loading is high (shown in Figure 1a), the AER  
 290 experiment produces 0.5 K to 1 K of warming relative to CTL. As dust travels off the west coast of Africa into the Atlantic,  
 291 the particles are lifted and carried by the Saharan Air Layer (SAL), around 800 – 600 hPa (Diaz et al., 1976; Karyampudi et  
 292 al., 1999). In the case of 12Z June 22, 2020, MERRA-2 captured the dust transport within SAL, and air mass is increasingly  
 293 composed of fine dust particles due to the gravitational settling of coarser particles (not shown here). Wei et al. (2021b)  
 294 conducted a series of CRTM v2.3 experiments using idealized dust profiles and reported that mass loading and the altitude of  
 295 the dust layer are the primary and secondary factors affecting the BT simulations, respectively; changes in the fine versus  
 296 coarse particle partition show little influence on the BT simulations. Based on these results we speculate that elevated dust  
 297 plume retains unneglected influences on BT calculations (Figure 3a). Experiments with robust estimated aerosol distributions  
 298 over extended time period are needed to quantify the sensitivity of GSI analysis to aerosol-aware CRTM calculations. This  
 299 manuscript, however, is intended to provide a joined-up documentation for the CRTM aerosol option and thus unravelling  
 300 these questions is beyond the scope of this study.

301

302

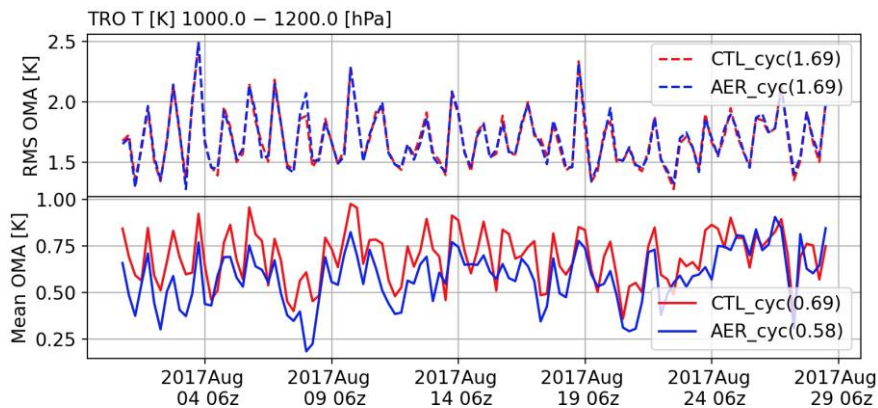


303  
 304 **Figure 5.** (a) The differences (AER - CTL) of analyzed temperature (K) at 900 hPa and (b) the corresponding aerosol column  
 305 mass density ( $\text{kg m}^{-2}$ ) from MERRA-2 on 12Z June 22, 2020.

### 306 3.2 Aerosol impacts on the analysis

307 The experiments reported in this section were produced with the NCEP GFS version 14 and the corresponding GDAS. Our  
 308 experiments used a coarser resolution, T670 ( $\sim 30$  km) for the model and T254 ( $\sim 80$  km) for the analysis, different from the  
 309 NCEP operational GFSv14 configuration at T1534 ( $\sim 13$  km) and T574 ( $\sim 27$  km). The experiments covered the August 2017  
 310 period, initialized from NCEP's archived GDAS analysis on July 25 00Z. The analysis cycles every 6 hours (at 00z, 06z, 12z,  
 311 and 18z), with a  $\pm 3$ -hour assimilation window and continuous data utilization. The control experiment (CTL\_cyc) was an  
 312 aerosol-blind fully cycled experiment where aerosol effects on radiances are not considered (as is by default). The aerosol  
 313 experiment (AER\_cyc) was an aerosol-aware fully cycled experiment where aerosol-affected satellite radiances are taken into  
 314 account. Here, we used CRTM version 2.2.4. Time-varying 3-dimensional GOCART aerosols were taken from NCEP's  
 315 archived NEMS GFS Aerosol Component (NGAC) v2 (Wang et al., 2018).

316  
 317 Figure 6 displays the statistics of analysis departures (observation minus analysis, OMA) from CTL\_cyc and AER\_cyc to  
 318 evaluate the performance of temperature analysis at the lower atmosphere over the tropical region ( $20^\circ \text{S} - 20^\circ \text{N}$ ). The positive  
 319 value of mean OMAs indicates that both experiments have cold biases in the tropical region. It shows neutral impact on root-  
 320 mean-square (RMS) and slightly positive impact on the cold biases. The latter implies that the departure of temperature analysis  
 321 becomes larger when considering aerosol transmittance effects during the data assimilation (i.e., AER\_cyc).



323

324 **Figure 6.** The comparison of the RMS and mean analysis departures (observation minus analysis, OMA) against in-situ  
 325 measurements (e.g., radiosonde) of temperature with pressure over 1,000 hPa at the tropical region (20° S – 20° N) during 00Z  
 326 August 1 – 18Z August 28, 2017.

327

328 Medium-range forecasts of AER\_cyc are examined against CTL\_cyc using the verification package from NOAA/NCEP EMC  
 329 ([https://www.emc.ncep.noaa.gov/gmb/STATS\\_vsdb](https://www.emc.ncep.noaa.gov/gmb/STATS_vsdb)). Figure 7 displays the scorecard of anomaly correlation and root-mean-  
 330 square error (RMSE) for the day-1, -3, and -5 forecasts over August 1 – 28, 2017. Anomaly correlation coefficients show  
 331 neutral to positive impact on day-1 forecasts of wind and temperature fields when aerosol cooling effects in BTs are considered.  
 332 The RMSE scorecards show the forecast improvements in the wind, temperature and height fields throughout the troposphere  
 333 over the Tropics (20° S – 20° N) and at upper level over the Northern Hemisphere (20° N – 80° N). For the Southern hemisphere  
 334 (20° S – 80° S), however, there is neutral impact or degradation in the forecasts, which is likely due to cloud contamination  
 335 and mixture of sea salt and aged smoke/sulfate aerosols. Compared to both hemispheres, the tropical forecasts show the most  
 336 improved statistics in the aerosol-aware analysis, which may be attributed to larger aerosol loading in this region. While the  
 337 RMSE scorecard focuses on background (i.e., time-averaged) fields, it should be noted that evaluation of the aerosol impacts  
 338 on the analysis and forecasts of African easterly wave that developed Hurricane Harvey and Gert in 2017 is presented in  
 339 Grogan et al. (2021).

340

			Globe			N. Hemisphere			S. Hemisphere			Tropics				
			Day 1	Day 3	Day 5	Day 1	Day 3	Day 5	Day 1	Day 3	Day 5	Day 1	Day 3	Day 5		
Anomaly Correlation	Heights	250hPa														
		500hPa														
		700hPa														
		1000hPa														
	Vector Wind	250hPa	▲													
		500hPa	▲													
		850hPa	▲													
	Temp	250hPa	▲													
		500hPa		▼												
		850hPa	▲													
RMSE	Heights	10hPa	▲	▲	▲		▲	▲	▲				▲	▲	▲	
		20hPa	▲	▲	▲	▲	▲	▲					▲	▲	▲	
		50hPa	▲	▲	▲	▲	▲	▲	▲	▲				▲	▲	▲
		100hPa	▲	▲	▲	▲	▲	▲	▲	▲				▲	▲	▲
		200hPa	▲											▲	▲	▲
		500hPa												▲	▲	▲
		700hPa														
		850hPa														
		1000hPa														
		Vector Wind	10hPa	▲	▲			▲	▲	▲					▲	▲
	20hPa		▲	▲			▲	▲	▲	▲	▲	▲		▲	▲	▲
	50hPa		▲	▲	▲	▲	▲	▲	▲	▲	▲	▲		▲	▲	▲
	100hPa		▲	▲	▲	▲	▲	▲	▲	▲	▲	▲		▲	▲	▲
	200hPa		▲				▲							▲	▲	
	500hPa		▲											▲	▲	
	700hPa		▲											▲	▲	
	850hPa		▲											▲	▲	
	1000hPa		▲											▲	▲	
	Temp		10hPa	▲	▲			▲							▲	▲
		20hPa	▲	▲			▲	▲	▲	▲	▲	▲		▲	▲	▲
		50hPa	▲	▲			▲	▲	▲	▲	▲	▲		▲	▲	▲
		100hPa	▲	▲	▲	▲	▲	▲	▲	▲	▲	▲		▲	▲	▲
		200hPa	▲				▲							▲	▲	▲
		500hPa														
		700hPa														
		850hPa	▲				▲							▲	▲	
		1000hPa	▲				▲							▲	▲	

341  
342 **Figure 7.** Scorecard of anomaly correlation and RMSE of comparison between AER\_cyc and CTL\_cyc. Green colors mean  
343 AER\_cyc is better than CTL\_cyc at 95% (filled box), 99% (▲), and 99.9% (▲) significance level. Red colors mean AER\_cyc  
344 is worse than CTL\_cyc at 95% (filled box), 99% (▼), and 99.9% (▼) significance level. Grey boxes mean no statistically  
345 significant difference between AER\_cyc and CTL\_cyc. Blue boxes are not statistically relevant. The statistics are calculated  
346 between 20 to 80 degrees of latitude for both hemispheres. The data between 20°S and 20°N is used for the tropical region.

347 **4. Conclusions and Future Outlook**

348 This article described aerosol absorption and scattering calculations of the CRTM version 2 in the GSI analysis. We also  
349 conducted sensitivity experiments to investigate the aerosol-affected GSI analysis in both single-cycle and fully-cycled runs.  
350 Both GSI and CRTM are well documented with user guides, tutorials and code repositories available online. This article is

351 primarily a joined-up documentation for aerosol absorption and scattering calculations in the CRTM version 2 and GSI. It also  
352 provides guidance for prospective users of the CRTM aerosol option. Scientific aspects of aerosol-affected BT in atmospheric  
353 data assimilation are briefly discussed. Specifically, numerical experiments were conducted to illustrate how including aerosol  
354 radiative effects in CRTM changes the GSI analysis. We found that taking the aerosols into account reduces simulated BT in  
355 thermal window channels over dust-dominant regions. Assimilating aerosol-affected BTs produces a warmer analyzed lower  
356 atmosphere. From the verification scorecard, neutral to positive results are found in the fully-cycled, aerosol aware experiment.

357  
358 The CRTM team, in coordination with its partners and collaborators, is building a robust capability to accurately and  
359 consistently simulate the emission, absorption, and scattering properties of all (radiatively important) atmospheric constituents.  
360 There are several ongoing and planned efforts to enhance the CRTM aerosol module. For example, more aerosol optical look-  
361 up tables have been added and the calculations of aerosol optical properties are being evaluated. In addition, the CRTM is  
362 being refactored toward a more flexible aerosol interface to handle aerosol optical look-up-tables as well as to support aerosol  
363 specifications from other operational aerosol models, such as Community Multiscale Air Quality (CMAQ). Other aerosol-  
364 related efforts include, but are not limited to, improving the physical representation of aerosols and including active sensors  
365 such as aerosol lidar. These developments, once implemented and tested, will be reported in future manuscripts.

#### 366 **Code and Data Availability.**

367 Various software packages are referred to throughout the paper. The following list contain links to the main software  
368 documentations or repositories discussed:

369 The GSI webpage: <https://dtcenter.ucar.edu/com-GSI/users/index.php>

370 The GSI v3.7 user guide: [https://dtcenter.ucar.edu/com-GSI/users/docs/users\\_guide/html\\_v3.7/index.html](https://dtcenter.ucar.edu/com-GSI/users/docs/users_guide/html_v3.7/index.html)

371 The GSI v3.7 online tutorial: [https://dtcenter.ucar.edu/com-GSI/users/tutorial/online\\_tutorial/index\\_v3.7.php](https://dtcenter.ucar.edu/com-GSI/users/tutorial/online_tutorial/index_v3.7.php)

372 The DTC community GSI (as of Nov. 29, 2021, via Zenodo): <https://doi.org/10.5281/zenodo.5735601>

373 The CRTM v2.3.0 public repository (via Zenodo): <https://doi.org/10.5281/zenodo.5695707>

374 The aerosol related Fortran code in GSI:

375 Aerosol files check (when `lread_ext_aerosol` is true): `./src/gsi/read_files.f90`

376 Aerosol data ingestion: `./src/gsi/ncepnmemo_io.f90`, `./src/gsi/general_read_nemsaero.f90`

377 CRTM simulation: `./src/gsi/crtm_interface.f90`

378 Effective radius setup: `./src/gsi/set_crtm_aerosolmod.f90`



379 **Author Contributions.**

380 QL implemented the aerosol module, CL designed the experiments, and SW performed the experiments. CL prepared the  
381 manuscript with contributions from all co-authors.

382 **Acknowledgements.**

383 The study of CTL and AER cycled experiments are supported by the Next Generation Global Prediction System (NGGPS)  
384 program within NOAA/NWS (award number 352 NA15NWS4680008). The testing and refinement of GSI/CRTM regression  
385 test is supported by the DTC Visitor Program. All experiments were conducted at NOAA/NESDIS-funded Supercomputer for  
386 Satellite Simulations and Data Assimilation Studies (S4) cluster maintained by Space Science and Engineering Center (SSEC)  
387 at University of Wisconsin-Madison. We thank GMAO collaborators, Arlindo da Silva, Mian Chin, and Peter Colarco, for  
388 providing valuable input on the calculations of aerosol optical properties for GOCART aerosols.

389 **References**

- 390 d'Almeida, G. A., Koepke, P., and Shettle, E.P.: Atmospheric Aerosols: global climatology and radiative characteristics, A.  
391 Deepak Publishing, Hampton, VA., 1991.
- 392 American Meteorological Society: Brightness Temperature. Glossary of Meteorology,  
393 [https://glossary.ametsoc.org/wiki/Brightness\\_temperature](https://glossary.ametsoc.org/wiki/Brightness_temperature), 2012.
- 394 Binkowski, F. S., Roselle, S. J.: Models-3 Community multiscale air quality (CMAQ) model aerosol component, 1 Model  
395 description. *J. Geophys. Res.*, 108, 4183, doi:10.1029/2001JD001409, 2003.
- 396 Buchard, V., da Silva, A. M., Colarco, P. R., Darmonov, A., Randles, C. A., Govindaraju, R., Torres, O., Campbell, J., and  
397 Spurr, R.: Using the OMI aerosol index and absorption aerosol optical depth to evaluate the NASA MERRA Aerosol  
398 Reanalysis. *Atmos. Chem. Phys.*, 15, 5743–5760, doi:10.5194/acp-15-5743-2015, 2015.
- 399 Bullard, J. E. and Coauthors: High-latitude dust in the Earth system, *Rev. Geophys.*, 54, 447–485, doi:10.1002/  
400 2016RG000518, 2016.
- 401 Chen, Y., Weng, F., Han, Y., and Liu, Q.: Planck-Weighted Transmittance and Correction of Solar Reflection for Broadband  
402 Infrared Satellite Channels. *J. Atmos. Sci.* 29, 382-396, 2012.
- 403 Chin, M., Ginoux, P., Kinne, S., Torres, O., Holben, B. N., Duncan, B. N., Martin, R. V., Logan, J. A., and Higurashi, A.:  
404 Tropospheric aerosol optical thickness from the GOCART model and comparisons with satellite and Sun photometer  
405 measurements, *J. Atmos. Sci.*, 59, 461–483, doi:10.1175/1520-0469(2002)059<0461:TAOTFT>2.0.CO;2, 2002.
- 406 Chin, M., Diehl, T., Tan, Q., Prospero, J. M., Kahn, R. A., Remer, L. A., Yu, H., Sayer, A. M., Bian, H., Geogdzhayev, I. V.,  
407 Holben, B. N., Howell, S. G., Huebert, B. J., Hsu, N. C., Kim, D., Kucsera, T. L., Levy, R. C., Mishchenko, M. I., Pan, X.,  
408 Quinn, P. K., Schuster, G. L., Streets, D. G., Strode, S. A., Torres, O., and Zhao, X.-P.: Multi-decadal aerosol variations

409 from 1980 to 2009: a perspective from observations and a global model, *Atmos. Chem. Phys.*, 14, 3657–3690,  
410 doi.org:10.5194/acp14-3657-2014, 2014.

411 Clough, S., Iacano, M. J. and Moncet, J.-L.: Line-by-line Calculations of Atmospheric Fluxes and Cooling Rates: Application  
412 to Water Vapor. *J. Geophys. Res.* 97, 15761-15785, 1992.

413 Colarco, P., da Silva, A., Chin, M., and Diehl, T.: Online simulations of global aerosol distributions in the NASA GEOS-4  
414 model and comparisons to satellite and ground-based aerosol optical depth, *J. Geophys. Res.*, 115, D14207,  
415 doi:10.1029/2009JD012820, 2010.

416 Diaz, H. F., Carlson, T. N., and Prospero, J. M.: A study of the structure and dynamics of the Saharan air layer over the northern  
417 equatorial Atlantic during BOMEX. National Hurricane and Experimental Meteorology Laboratory NOAA Tech. Memo.  
418 ERL WMPO-32, 61 pp, 1976.

419 Diaz, J. P., Arbelo, M., Expósito, F.J., Podesta', G., Prospero, J.M., and Evans, R.: Relationship between errors in AVHRR-  
420 derived sea surface temperature and the TOMS Aerosol Index, *Geophys. Res. Lett.*, 28, 1989 – 1992, 2001.

421 Divakarla, M., and Coauthors: Evaluation of CrIMSS operational products using in-situ measurements, model analysis fields,  
422 and retrieval products from heritage algorithms, IEEE International Geoscience and Remote Sensing Symposium, Munich,  
423 Germany, 2012, pp. 1046-1049, doi: 10.1109/IGARSS.2012.6350818, 2012.

424 Gelaro, R., McCarty, W., Suarez, M. J., Todling, R., and coauthors, 2017: The Modern-Era Retrospective Analysis for  
425 Research and Applications, Version 2 (MERRA-2). *J. Climate*, 30, 5419–5454, doi.org: 10.1175/JCLI-D-16-0758.1, 2017.

426 Grogan, D., Lu, C.-H., Wei, S.-W., and Chen, S.-P.: Effects of Saharan dust on African easterly waves: The impact of aerosol-  
427 affected satellite radiances on data assimilation, *Atmos. Chem. Phys. Disc.*, doi:10.5194/acp-2021-129, 2021.

428 Hale, G. M. and Querry, M. R.: Optical constants of water in the 200-nm to 200-mm wavelength region. *Appl. Opt.*, 12, 555–  
429 563, 1973.

430 Han, Y., van Delst, P., Liu, Q., Weng, F., Yan, B., Treadon, R., and Derber, J.: JCSDA Community Radiative Transfer Model  
431 (CRTM) – Version 1, NOAA NESDIS Tech. Rep. 122, 33 pp., NOAA, Silver Spring, Md, 2006.

432 Han, Y., Weng, F., Liu, Q., and van Delst, P.: A fast radiative transfer model for SSMIS upper atmosphere sounding channels.  
433 *J. Geophys. Res.*, 112, D11121, doi:10.1029/2006JD008208, 2007.

434 Hess, M., Koepke, P., Schult I: Optical properties of aerosols and clouds: the software package 1528 OPAC. *Bull Am Met Soc*  
435 79:831–844, 1998.

436 Highwood, E. J., Haywood, J. M., Silverstone, M. D., Newman, S. M., and Taylor, J. P.: Radiative properties and direct effect  
437 of Saharan dust measured by the C-130 aircraft during Saharan Dust Experiment (SHADE): 2. Terrestrial spectrum, *J.*  
438 *Geophys. Res.*, 108(D18), 8578, doi:10.1029/2002JD002552, 2003.

439 Karyampudi, V. M., Palm, S. P., Reagen, J. A., Fang, H., Grant, W. B., Hoff, R. M., Moulin, C., Pierce, H.  
440 F., Torres, O., Browell, E. V., and Melfi, S. H.: Validation of the Saharan dust plume conceptual model using lidar,  
441 Meteosat, and ECMWF data, *Bull. Am. Meteorol. Soc.*, 80, 1045–1075, doi:10.1175/1520-  
442 0477(1999)080<1045:VOTSDP>2.0.CO;2.

443 Kim, J., Akella, S., da Silva, A.M., Todling, R., McCarty, W.: Preliminary evaluation of influence of aerosols on the simulation  
444 of brightness temperature in the NASA's Goddard Earth Observing System Atmospheric Data Assimilation System; Tech.  
445 Rep. Ser. Glob. Model. Data Assim., Vol 49, TM-2018-104606, Goddard Space Flight Center, National Aeronautics and  
446 Space Administration: Greenbelt, Maryland, US, 2018.

447 Kleist, D. T., Parrish, D. F., Derber, J. C., Treadon, R., Wu, W. S., and Lord, S.: Introduction of the GSI into the NCEP Global  
448 Data Assimilation System. *Weather and Forecasting*, 24(6):16911705, 2009.

449 Letertre-Danczak, J.: The Use of Geostationary Radiance Observations at ECMWF and Aerosol Detection for Hyper-Spectral  
450 Infrared Sounders: 1st and 2nd Years Report; EUMETSAT/ECMWF Fellowship Programme Research Reports, Vol 40,  
451 European Centre for Medium Range Weather Forecasts: Shinfield Park, Reading, RG2 9AX, England, 2016.

452 Liu, Q. and Weng, F.: Advanced doubling-adding method for radiative transfer in planetary atmosphere, *J. Atmos. Sci.*, 63,  
453 3459-3465, doi:10.1175/JAS3808.1, 2006.

454 Liu, Q., Han, Y., van Delst, P., and Weng, F.: Modeling aerosol radiance for NCEP data assimilation, in *Fourier Transform  
455 Spectroscopy/Hyperspectral Imaging and Sounding of the Environment*, paper HThA5, OSA Technical Digest Series,  
456 Optical Society of America, doi:10.1364/HISE.2007.HThA5, 2007.

457 Liu, Q. and Lu, C.-H.: Community Radiative Transfer Model for Air Quality Studies. In *Light Scattering Reviews*. 456  
458 Kokhanovsky, A., Eds.; Springer Praxis Books, Springer-Verlag, Berlin – Heidelberg, Germany, Volume 457, pp. 67-115,  
459 2016.

460 Liu, Z., Liu, Q., Lin, H.-C., Schwartz, C. S., Lee, Y.-H., and Wang, T.: Three-dimensional variational assimilation of MODIS  
461 aerosol optical depth: Implementation and application to a dust storm over East Asia, *J. Geophys. Res.*, 116, D23206,  
462 doi:10.1029/2011JD016159, 2011.

463 Lu, C.-H., da Silva, A., Wang, J., Moorthi, S., Chin, M., Colarco, P., Tang, Y., Bhattacharjee, P. S., Chen, S.-P., Chuang, H.-  
464 Y., Juang, H.-M. H., McQueen, J., and Iredell, M.: The implementation of NEMS GFS Aerosol Component (NGAC)  
465 version 1.0 for global dust forecasting at NOAA/NCEP, *Geosci. Model Dev.*, 9, 1905–1919, doi: 10.5194/gmd-9-1905-  
466 2016, 2016.

467 Matricardi, M.: The inclusion of aerosols and clouds in RTIASI, the ECMWF fast radiative transfer model for the infrared  
468 atmospheric sounding interferometer, *ECMWF Tech. Memo.*, 474, doi: 10.21957/1krvb28ql, 2005.

469 Merchant, C. J., Embury, O., Le Borgne, P. and Bellecm B.: Saharan dust in nighttime thermal imagery: Detection and  
470 reduction of related biases in retrieved sea surface temperature, *Remote Sensing of Environ.*, 104, 15–30, doi:  
471 10.1016/j.rse.2006.03.007, 2006.

472 Nalli, N. R., and L. L. Stowe, Aerosol correction for remotely sensed sea surface temperatures from the National Oceanic and  
473 Atmospheric Administration advanced very high resolution radiometer, *J. Geophys. Res.*, 107(C10), 3172, doi:10.1029/  
474 2001JC001162, 2002.

475 Pagowski, M., Liu, Z., Grell, G. A., Hu, M., Lin, H.-C., Schwartz, C. S., Implementation of aerosol assimilation in Gridpoint  
476 Statistical Interpolation (v3.2) and WRF-Chem (v.3.4.1), *Geosci. Model Dev.*, 7, 1621–1627, doi:10.5194/gmd-7-1621-  
477 2014, 2014.

478 Petty G: A First Course in Atmospheric Radiation, 2nd edition, Sundog Publishing, Madison, WI, 2006.

479 Peyridieu, S., Chdin, A., Tanr, D., Capelle, V., Pierangelo, C., Lamquin, N., and Armante, R.: Saharan dust infrared optical  
480 depth and altitude retrieved from AIRS: a focus over North Atlantic comparison to MODIS and CALIPSO, *Atmos. Chem.*  
481 *and Phys. Discuss.*, 9(5):2119921235, 2009.

482 Pierangelo, C., Chedin, A., Heilliette, S., Jacquinet-Husson, N., and R. Armante, R.: Dust altitude and infrared optical depth  
483 from AIRS. *Atmos. Chem. Phys.*, 4, 1813-1822, doi: 10.5194/acp-4-1813-2004, 2004.

484 Randles, C. A., da Silva, A. M., Buchard, V., Colarco, P. R., Darmenov, A., Govindaraju, R., Smirnov, A., Holben, B., Ferrare,  
485 R., Hair, J., Shinozuka, Y., Flynn, C., J: The MERRA-2 Aerosol Reanalysis, 1980 Onward. Part I: System Description and  
486 Data Assimilation Evaluation, *Journal of Climate*, 30(17), 6823-6850, doi:10.1175/JCLI-D-16-0609.1, 2017.

487 Schwartz, C. S., Liu, Z., Lin, H.-C., and Cetola, J. D.: Assimilating aerosol observations with a “hybrid” variational-ensemble  
488 data assimilation system, *J. Geophys. Res.-Atmos.*, 119, 4043–4069, doi:10.1002/2013JD020937, 2014.

489 Sokolik, I. N.: The spectral radiative signature of wind-blown mineral dust: Implications for remote sensing in the thermal IR  
490 region: The spectral radiative signature of wind-blown mineral dust, *Geophys. Res. Lett.*, 29, 7-1-7-4,  
491 doi:10.1029/2002GL015910, 2002.

492 Stegmann, P. G., Tang, G., Yang, P. and Johnson, B. T.: A stochastic model for density-dependent microwave Snow- and  
493 Graupel scattering coefficients of the NOAA JCSDA community radiative transfer model, *J. Quant. Spec. Rad. Trans.*,  
494 211, 9-24, doi:10.1016/j.jqsrt.2018.02.026, 2018.

495 Ukhov, A., Ahmadov, R., Grell, G., and Stenchikov, G.: Improving dust simulations in WRF-Chem model v4.1.3 coupled  
496 with GOCART aerosol module, *Geosci. Model Dev. Disc.*, doi:10.5194/gmd-2020-92, 2021.

497 Wang, J., Bhattacharjee, P.S., Tallapragada, V., Lu, C.-H., Kondragunta, S., da Silva, A., Zhang, X., Chen, S.-P., Wei, S.-W.,  
498 Darmenov, A.S., et al.: The implementation of NEMS GFS Aerosol Component (NGAC) Version 2.0 for global  
499 multispecies forecasting at NOAA/NCEP – Part 1: Model descriptions., *Geosci. Model Dev.*, 11, 2315–2332,  
500 doi:10.5194/gmd-11-2315-2018, 2018.

501 Weaver, C. J., Joiner, J., and Ginoux, P.: Mineral aerosol contamination of TIROS Operational Vertical Sounder (TOVS)  
502 temperature and moisture retrievals., *J. Geophys. Res.*, 108, doi:10.1029/2002JD002571, 2003.

503 Wei, S.-W., Lu, C.-H., Liu, Q., Collard, A., Zhu, T., Grogan, D., Li, X., Wang, J., Grimbine, R., and Bhattacharjee, P.: The  
504 impact of aerosols on satellite radiance data assimilation using NCEP global data assimilation system, *Atmos.*, 12(4), 432,  
505 doi:10.3390/atmos12040432, 2021a.

506 Wei, S.-W., Lu, C.-H., Johnson, B. T., Dang, C., Stegmann, P., Grogan, D., Ge, G., and Hu, M.: The influence of aerosols on  
507 satellite infrared radiance simulations and Jacobians: Numerical experiments of CRTM and GSI, *Remote. Sens.*, in review,  
508 2021b.

509 Weng, F.: Advances in radiative transfer modeling in support of satellite data assimilation. *J. Atmos. Sci.*, 64, 3799–3807,  
510 doi:10.1175/2007JAS2112.1, 2007.

511 Wu, W.-S., Purser, R. J., and Parrish, D. F.: Three-dimensional variational analysis with spatially inhomogeneous covariances,  
512 *Mon. Weather Rev.*, 130, 2905–2916, doi:10.1175/1520-0493(2002)130<2905:TDVAWS>E2.0.CO;2, 2002.

513 Wu, M., Liu, X., Yu, H., Wang, H., Shi, Y., Yang, K., Darmenov, A., Wu, C., Wang, Z., Luo, T., Feng, Y., and Ke, Z.:  
514 Understanding processes that control dust spatial distributions with global climate models and satellite observations,  
515 *Atmos. Chem. Phys.*, 20, 13835–13855, <https://doi.org/10.5194/acp-20-13835-2020>, 2020.

516 Zhang L., Grell, G.A., Montuoro, R., McKeen, S. A., Bhattacharjee, P. S., Baker, B., Henderson, J., Pan, L., Frost, G. J.,  
517 McQueen, J., Saylor, R., Ahmadov, R., Li, H., Wang, J., Stajner, I., Kondragunta, S., Zhang, X., Li, F.: Development of  
518 GEFS-Aerosols into NOAAs Unified Forecast System UFS., *Geosci. Model Dev. Discuss.*, doi:10.5194/gmd-2021-378,  
519 2021.